Received January 23 2025, accepted July 12 2025, date of publication September 22 2025.

Original Research Article

Influence of Airflow on Dispersion of COVID-19 Droplets in Classrooms Using Computational Fluid Dynamics

Asisha Ranjan Pradhan[1], Shivam Kumar[2,3], Agus Saptoro[4], Perumal Kumar[4], Jono Suhartono[5], Satish Kumar[3], and Jashanpreet Singh[6,*]

[1] Indian Institute of Technology Hyderabad, Telangana, India.
[2] WA School of Mines: Minerals, Energy and Chemical Engineering, Curtin University, Perth, Australia.
[3] National Institute of Technology, Jamshedpur, Jharkhand, India.
[4] Curtin University, Sarawak, Malaysia.
[5] Institut Teknologi Nasional Bandung, Indonesia.
[6] University Centre for Research and Development, Chandigarh University, Mohali, Punjab, India.

[*] Corresponding Author Email: ijashanpreet@gmail.com

ABSTRACT

COVID-19, caused by the 2019-nCoV coronavirus, is a global pandemic that spreads through respiratory droplets that are transmitted by inhalation or contact with droplet nuclei produced during sneezing, coughing, and speaking by infected people. COVID-19 can also be spread by air in the infected person's close-by surroundings. In this study, computational fluid dynamics (CFD) was employed to analyze the airborne transport of virus-laden droplets generated by a coughing event in a typical classroom environment. Simulations were conducted for three ventilation airflow velocities—3, 5, and 7 m/s—under both side and top wall configurations. The results showed that higher airflow velocities significantly reduced the residence time of airborne particles, with the 7 m/s case clearing over 90% of droplets within 60 seconds. Top wall ventilation led to early dispersion near the front rows, while side wall ventilation carried droplets to the rear seats over time. In addition, smaller aerosols (< 1 μm) remained suspended for a significantly longer duration than larger droplets (> 100 μm), indicating higher long-range transmission risk. These findings underscore the importance of optimizing airflow velocity and vent placement to reduce airborne exposure and support safer classroom ventilation design.

Keywords—*COVID-19, Classroom, CFD, Airborne transmission, Ventilation.*

INTRODUCTION

COVID-19 is a highly contagious respiratory illness caused by the 2019-nCoV coronavirus, which belongs to the destructive coronavirus family that has rapidly spread worldwide, resulting in a pandemic.[1–3] Airborne transmission involves inhaling virus-laden aerosols, which are smaller than 5 μm. These aerosols can travel in airflows and infect individuals at short and long distances from the source.[4–6] These droplet nuclei are created when infected individuals sneeze, cough, or talk. Individuals' social, cognitive, and intellectual development is greatly enhanced by classrooms.[7] However, because of many uncertainties about the transmission routes of COVID-19, there are ongoing worries about creating safe and supportive educational settings. Environmental factors such as temperature, humidity, and ventilation significantly affect the transmission of aerosols. Poorly ventilated indoor spaces increase the risk of airborne transmission.[4,5,8] One crucial question that requires attention is how the ventilation systems in the classroom impact the ability of the virus to spread. Computational fluid dynamics (CFD) can simulate the propagation of virus-laden droplets from an infected student's sneezing or coughing to avoid experimental complications.[9–11] Statistical investigations showed that COVID-19 dispersed by aerosols, droplets, fomites, and human waste affected human health.[12,13] Asadi et al. investigated the spread of COVID-19 by direct or indirect contact, including transmission through the air when sneezing or coughing and through physical contact with contaminated objects.[14] Diwan et al. investigated the airflow produced by sneezing and coughing in dry and wet circumstances.[15] They also considered the evaporation of droplets using direct numerical simulations (DNS). The researchers replicated the act of coughing by modelling it as a turbulent jet/puff phenomenon. Kotb and Khalil used ANSYS-Fluent 18.0 to mimic COVID-19 transmission by sick passengers sneezing and coughing in an aircraft cabin.[16] They found that sneeze droplets were more harmful than cough droplets, yet both could travel long distances in the aircraft. As speed rises, more droplets are distributed. Wang et al. calculated the distribution of COVID-19-contaminated particles from sneezing in a three-bed hospital unit.[17] Particle path and residency period were simulated using ANSYS Fluent 19.0 to assess cross-infection risk.

Common ventilation systems change indoor air concentration, temperature, and humidity.[18,19] The influence of displacement and mixed ventilation systems on interior air quality affects human health and comfort.[20,21] Multiple studies show that poor ventilation increases disease transmission in confined settings. Several researchers have studied indoor airflow, room pressurization, and filtration in infectious illness hospitals and chemical labs.[22,23] The goal was to find low-risk situations. Ren et al. numerically modelled three typical breathing strategies in a hospital's prefabricated COVID-19 inpatient room.[24] The study examined various droplet sizes. Main currents transport small particles across significant distances. Portions of droplets are expelled via outlet ventilation. However, streams cannot carry large particles. They land on solid objects because of gravity. Different ventilation methods cause sedimentation in different parts of the ward.

Because of the lack of empirical data on COVID-19-infected droplet fluid dynamics, models of droplet transmission by sneezing or coughing are useful.[25,26] This analysis improves our understanding of the COVID-19 simulation. Gupta et al. experimentally studied coughing airflow dynamics.[27] Researchers used gamma functions to track coughing rates throughout time. The researchers found no association between cough direction, mouth opening size, and physiological parameters, including height, weight, and gender. Many studies show how human-breathed air affects respiratory infections in ventilated environments to minimize breathing-related infections.[28,29] Big droplets settle swiftly over a short distance and are hardly affected by air temperature changes. However, personal contact with an infected person might spread droplet-borne diseases to susceptible others. Educational researchers have examined COVID-19 transmission among pupils. Abuhegazy et al. studied COVID-19 aerosol mobility and deposition on classroom surfaces.[30] They found that particle size, aerosol source location, glass barriers, and windows affected their numerical results. The researchers found that gravitational sedimentation deposits bigger particles on the ground, tables, and other surfaces in the room, whereas the air conditioning system expels most small particles. Researchers have studied seat placement in different rooms and regions using equilateral triangle seat designs.[31] Their COVID-19 study may benefit schools, universities, restaurants, libraries, and other indoor areas

where seat availability is crucial. This method boosts seats by 13% on average and 25% to 50% sometimes.

The review of the existing sources and the consistency of concerns and uncertainties regarding the COVID-19 spread demonstrate the necessity for further studies on the distribution of the virus in the classroom. It is important to develop suitable design methods to reduce the risk of air transmission within these environments. This paper has applied CFD to study the geographical and time dispersion of virus-laden droplets emitted by a coughing individual in a typical classroom. The paper examines how the velocities of airflow ventilation and droplet sizes affect the dispersion of infectious particles and how sitting positions are more vulnerable to infection. The originality of this study lies in the extensive modelling of aerosol-sized and large ballistic droplet behavior within an authentic classroom layout under the various ventilation types, which helps in gaining useful information on how to improve airflow and counter the issues of transmission indoors.

MATHEMATICAL MODEL

In this investigation, numerical modelling of the flow dynamics of the transmission of the COVID-19 virus was done using the RNG k-e model in Ansys Fluent 19.0. The Eulerian–Lagrangian approach was used to monitor the water droplets of different sizes released from the mouth of the diseased individual standing in front of the classroom because of coughing.

Ventilation Airflow Modelling

The equations (1–3) that describe the preservation of mass, momentum, and energy for a steady airflow that does not change in volume are as follows:

$$\frac{\partial \rho}{\partial t} + \nabla \cdot \left(\rho \vec{V} \right) = 0 \tag{1}$$

$$\rho \left(\frac{\partial \vec{V}}{\partial t} + \vec{V} \cdot \nabla \vec{V} \right) = -\nabla P + \mu \nabla^2 \vec{V} + \vec{S} \tag{2}$$

$$\rho \frac{\partial T}{\partial t} + \rho \vec{\nabla} \cdot \left(T \vec{V} \right) = \nabla \cdot \left(\frac{K}{C_p} \nabla T \right) + S_T \tag{3}$$

where, ρ is the Fluid density (kg/m^3), t is the time (s), $\vec{V}$ is the Velocity vector field (m/s), and $\nabla \cdot (\rho \vec{V})$ is the divergence of mass flux. In equation (2), the P denotes the pressure (Pa), μ denotes the dynamic viscosity (Pa·s), $\nabla^2 \vec{V}$ denotes the Laplacian of velocity (diffusion of momentum), and $\vec{S}$ denotes the external source term (e.g., body forces like gravity or electromagnetic forces). In equation (3), T is the temperature (K), K is the thermal conductivity (W/m·K), C_p is the specific heat capacity at constant pressure (J/kg·K), and the $\nabla \cdot \left(\frac{K}{C_p} \nabla T \right)$ is the heat diffusion term, and S_T is the volumetric heat source (e.g., radiation, chemical reaction, Joule heating).

Turbulence Modelling

According to Tsan–Hsung, the RNG k-ε turbulence model is a reasonable choice for modelling airflow in interior conditions.[32] The dissipation rate ε and turbulent kinetic energy k have matching transport equations, which are given as:

$$\frac{\partial}{\partial t}(\rho k) + \frac{\partial}{\partial x_i}(\rho k u_i) = \frac{\partial}{\partial x_j}\left[\alpha_k \quad \mu_{eff} \quad \frac{\partial k}{\partial x_j} \right] + G_k - \rho \varepsilon + S_k \tag{4}$$

$$\frac{\partial}{\partial t}(\rho \varepsilon) + \frac{\partial}{\partial x_i}(\rho \varepsilon u_i) = \frac{\partial}{\partial x_j}\left[\alpha_\varepsilon \quad \mu_{eff} \quad \frac{\partial \varepsilon}{\partial x_j} \right] + C_{1\varepsilon} \frac{\varepsilon}{k}(G_k) - C_{2\varepsilon} \rho \frac{\varepsilon^2}{k} - R_\varepsilon + S_\varepsilon \tag{5}$$

where, G_k represents the turbulent kinetic energy output resulting from the average velocity gradients. In this context, S_ε and S_k represent source terms that are defined by the user, while refers to the source term derived by renormalization. The x_i and x_j represent the i^{th} and j^{th} spatial coordinates, respectively. The Equations (4) and (5) define α_k and α_ε as the effective inverse Prandtl numbers for the turbulent kinetic energy and its dissipation, respectively. The symbol ε represents the turbulence dissipation rate ($m2/s3$), μ_{eff} is the effective viscosity, and u_i is the velocity component in x_i-direction. The product $\rho\varepsilon$ represents the dissipation of turbulent kinetic energy (k) into heat. The model constants $C_{1\varepsilon}$ and $C_{2\varepsilon}$ are assigned the values of 1.42 and 1.68, respectively.

Discrete Phase Modelling

In this study, the airflow was initially assessed for a sparse concentration of droplets before analyzing the trajectory of particles. The movement of droplets carrying viruses was examined employing Newton's second law within a Lagrangian framework,[33–35] with the associated equation of motion expressed as:

$$\frac{d\vec{V}_d}{dt} = F_D\left(\vec{V} - \vec{V}_d\right) + \frac{\vec{g}\left(\rho_d - \rho\right)}{\rho_d} + F_L + F_B \quad (6)$$

In Equation (6), F_L represents the Saffman lift force, and F_B denotes the Brownian force[36]. The given equation is the Lagrangian particle force balance used in multiphase flow modeling, where $\frac{d\vec{V}_d}{dt}$ denotes the acceleration of the dispersed particle with $\vec{V}_d$ as its velocity. The term $F_D\left(\vec{V} - \vec{V}_d\right)$ represents the drag force per unit particle mass, where $\vec{V}$ is the fluid velocity and F_D is the drag coefficient depends on Reynolds number and drag law. The term $\frac{\vec{g}\left(\rho_d - \rho\right)}{\rho_d}$ accounts for gravitational and buoyancy effects, with $\vec{g}$ being gravitational acceleration, ρ_d the particle density, and ρ the fluid density; this drives particles to settle if $\rho_d > \rho$ or rise if $\rho_d < \rho$. While F_D represents the coefficient of drag force. given as (Equations 7 and 8):

$$F_D = \frac{18\mu}{d^2 \rho_d C_c} \quad (7)$$

$$C_c = 1 + \frac{2K}{d}\left(1.257 + 0.4e^{-\left(\frac{1.1d}{2K}\right)}\right) \quad (8)$$

where, μ is the fluid's dynamic viscosity, d is the particle diameter, ρ_d is the particle density, and C_C is the Cunningham correction factor that corrects drag at very small particles.[37,38] Within the Cunningham coefficient, the ratio $2\lambda/d$ appears, where λ is the mean free path of gas molecules, which introduces a slip correction when particles are comparable in size to the molecular spacing. The mass flow rate of particles is expressed as (Equation 9):

$$\dot{m} = \frac{\left(\frac{4}{3}\pi r^3\right) \times \rho_d \times n}{t} \quad (9)$$

where, the symbol $\dot{m}$ denotes the particle mass flow rate, representing the mass of particles transported per unit time. Symbols n and ρ represent the number and density of particles, respectively. The ρ_d is the particle material density used in determining individual particle mass and flow contributions

In Equation 10, F_L represents the Saffman lift force, given as:

$$F_L = 6.46\mu_f \left(\frac{d_p}{2}\right)^1 V_s \left(\frac{\rho_f G}{\mu_f}\right)^{\frac{1}{2}} \quad (10)$$

where, d_p represents the mean diameter of particles, μ_f is the dynamic viscosity of the fluid, and V_s is the slip velocity defined as the relative velocity between the fluid and the particle. The term ρ_f represents the fluid density, while G denotes the velocity gradient in the surrounding fluid.

Geometry

This study has examined the movement and scattering of droplets that carry the COVID-19 virus produced by coughing in a classroom with under-ventilated or non-ventilated circumstances. The dimensions and specifications of the classroom and chairs are depicted in Figure 1 (a) and Figure 1 (b) from both a top perspective and a side view.

The classroom floor under study dimensions is 6 m in width and 8 m in length. The height of the classroom is 4.5 m. The floor area per student is consistent with a value of 0.36 square m. The class's student seating is arranged with a precise distance of 0.5 m. Figure 2 displays a comprehensive 3D representation of the simulated classroom, including all relevant details.

This study examines the scenario where an individual infected with COVID-19, measuring 1.8 m in height and with a mouth area of 4 cm^2, coughs abruptly and releases virus-infested droplets into the surrounding environment. The ventilation air is drawn in from a wall intake located behind and on top of the individual and is expelled via the open door. The door dimension is 1 × 2.1 m^2.

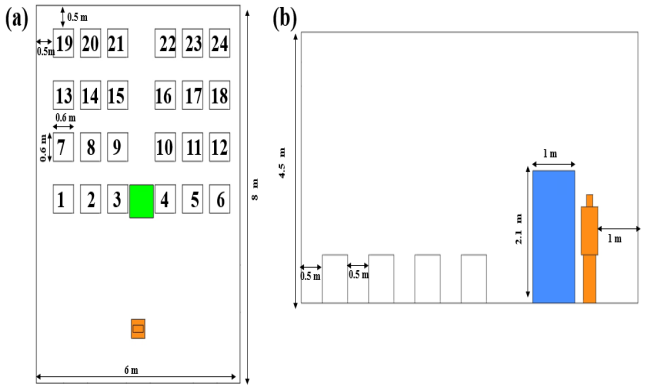

FIGURE 1. Classroom geometry and schematics. (a) Top view. (b) Side view.

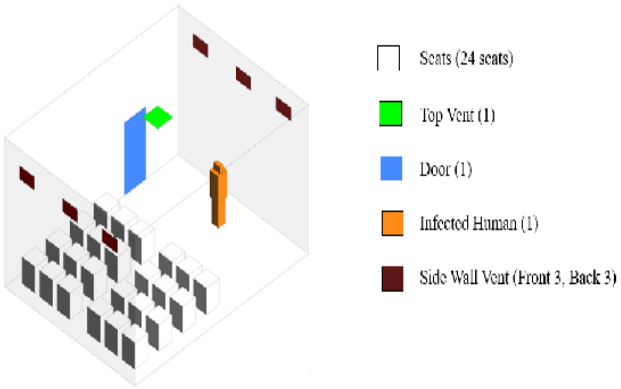

FIGURE 2. 3D model of the classroom with all the details.

Meshing

All simulations use an unstructured tetrahedral mesh created with ANSYS-Fluent, as shown in Figure 3. Meshing details are provided in Table 1.

Boundary Conditions and Solution Process

The simulations are conducted for both scenarios: one without and one with ventilation. The ventilation was positioned in several locations, including top ventilation, side wall ventilation with either one or three ventilation apertures, and the classroom door was used as the exit for the ventilation. Water droplets of different sizes are analyzed to represent the current conditions accurately. A coughing velocity of 10 m/s sustained for 0.75 seconds was applied, in alignment with measured human coughing dynamics reported by Gupta et al.[27] The injected droplet diameters ranged from 0.15 μm to 150 μm, consistent with experimental respiratory emission size distributions.[30] Inlet velocities of 3, 5, and 7 m/s and the corresponding outlet placements were selected based on airflow conditions investigated in previous classroom ventilation studies.[16] The specific details of the droplets are provided in Table 2.

Boundary Conditions and Solution Process

The simulations are conducted for both scenarios: one without and one with ventilation. The ventilation was positioned in several locations, including top ventilation, side wall ventilation with either one or three ventilation apertures, and the classroom door was used as the exit for the ventilation. Water droplets of different sizes are analyzed to represent the current conditions accurately. A coughing velocity of 10 m/s sustained for 0.75 seconds was applied, in alignment with measured human coughing dynamics reported by Gupta et al.[27] The injected droplet diameters ranged from 0.15 μm to 150 μm, consistent with experimental respiratory emission size distributions.[30] Inlet velocities of 3, 5, and 7 m/s and the corresponding outlet placements were selected based on airflow conditions investigated in previous classroom ventilation studies.[16] The specific details of the droplets are provided in Table 2.

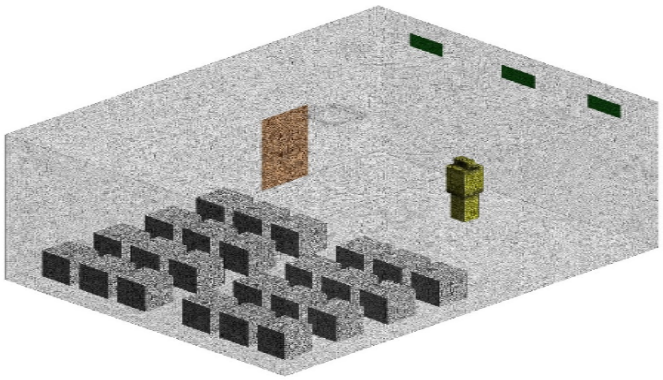

FIGURE 3. Meshing of the flow domain.

TABLE 1. Meshing details.

Parameter	Value
Cell type	Tetrahedrons
Maximum face size	50 mm
Nodes	672,869
Elements	3,679,749
Skewness	0.21935
Orthogonal quality	0.77935
Aspect ratio	1.8284

TABLE 2. Injection conditions for droplets carrying COVID-19 viruses.

Diameter (µm)	Velocity (m/s)	Number of Particles	Injection Time (Sec)	Mass Flow Rate (kg/sec)
0.15	10	1,800	0.75	4.2413E-15
1	10	1,800	0.75	1.2566E-12
10	10	1,800	0.75	1.2566E-09
50	10	1,800	0.75	1.5706E-07
100	10	1,800	0.75	1.2566E-06
150	10	1,800	0.75	4.2413E-06

The trap condition is used for the solid walls to govern the interactions between droplets and various surfaces, while the escape condition is utilized for the inlet and exit. The simulation utilizes three velocities within this range and subsequently compares the outcomes. The additional boundary conditions employed include a velocity input and a pressure exit. The temperature is set as a starting value for the outlet. In addition, a turbulence intensity of 5% is assumed at the inlet.

RESULT

This section delineates the numerical validation and results derived from CFD simulations, emphasizing airflow dynamics, turbulence intensity, and particle dispersion across varying droplet sizes and airflow velocities under distinct ventilation setups.

Validation

Prior to analyzing the fluid dynamics and flow patterns within the classroom geometry, the current numerical model for simulating particle motion was validated against the results of Jacob et al.[39] Figure 4(a) illustrates the computational domain, while Figure 4(b) presents the velocity profiles at various locations within the designed room. In addition, Figure 4(c) compares the velocity distributions at different locations, demonstrating a strong agreement with the findings from the previous study.

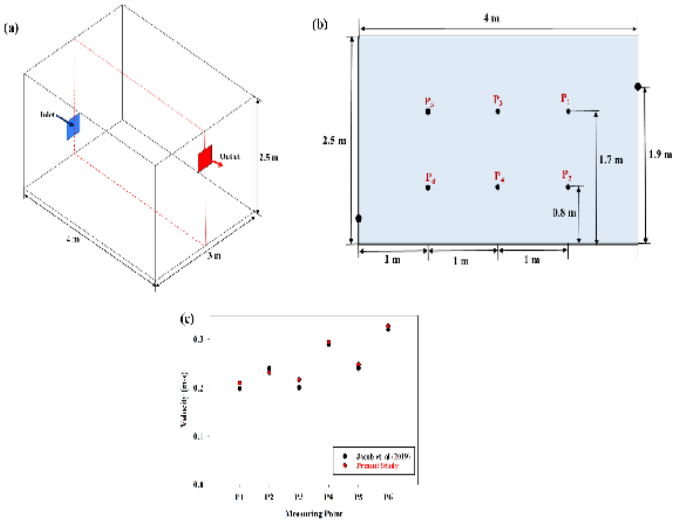

FIGURE 4. (a) Computational domain for validation, (b) measured location inside the test chamber, and (c) velocity distribution at various positions.

Airflow Characteristics

The airflow distribution within the classroom was simulated under different ventilation configurations (top and side walls) and inlet velocities (3 m/s, 5 m/s, and 7 m/s). The velocity distribution analysis within the classroom was carried out concerning different airflow velocities (3, 5, and 7 m/s) and two ventilation patterns: side wall and top wall ventilation. Figure 5 demonstrates that side wall ventilation creates a horizontal jet that becomes deeper and larger in circulation as velocity augments and circulation zones influence particle movement and dispersion. The recirculation zone is clear-cut and increases with the inlet velocities. As velocity increases, the graph in Figure 6 demonstrates a rise throughout the room. Contrarily, Figure 7 presents velocity vector fields at the mid-plane for top wall ventilation across three inletvelocities—3, 5, and 7 m/s—demonstrating the formation of

a downward airflow jet from the ceiling. Figure 8 shows the corresponding velocity magnitude contours near the floor, indicating that at the highest velocity of 7 m/s, the airflow penetrates more deeply into the student seating area, thereby increasing airflow coverage near occupant breathing zones.

Turbulence Intensity Distribution

An analysis of turbulence kinetic energy (TKE) was conducted to examine the influence of airflow velocity on turbulent mixing in the classroom. TKE contours illustrate the impact of ventilation airspeed on turbulent mixing. The results demonstrate a clear association between input airspeed and the magnitude and intensity of turbulent regions. In side ventilation (Figure 9), an increase in inflow velocity results in a wider and more violent turbulence zone. The top wall ventilation (Figure 10) demonstrates elevated turbulent kinetic energy (TKE) next to the first row of students and the droplet source, indicating enhanced mixing in the anterior area.

Droplet Size and Settling Behavior

Figure 11 illustrates the dynamic behavior of droplets of varying diameters 1 s after a coughing event simulated with a velocity of 10 m/s sustained for 0.75 s. Larger and heavier droplets, such as those measuring 100 µm and 150 µm, exhibit rapid gravitational settling as expected, while smaller droplets measuring less than 1 µm remain suspended in the air for a prolonged duration. This persistence highlights their potential role as aerosol carriers, contributing to airborne transmission risk within the classroom environment.

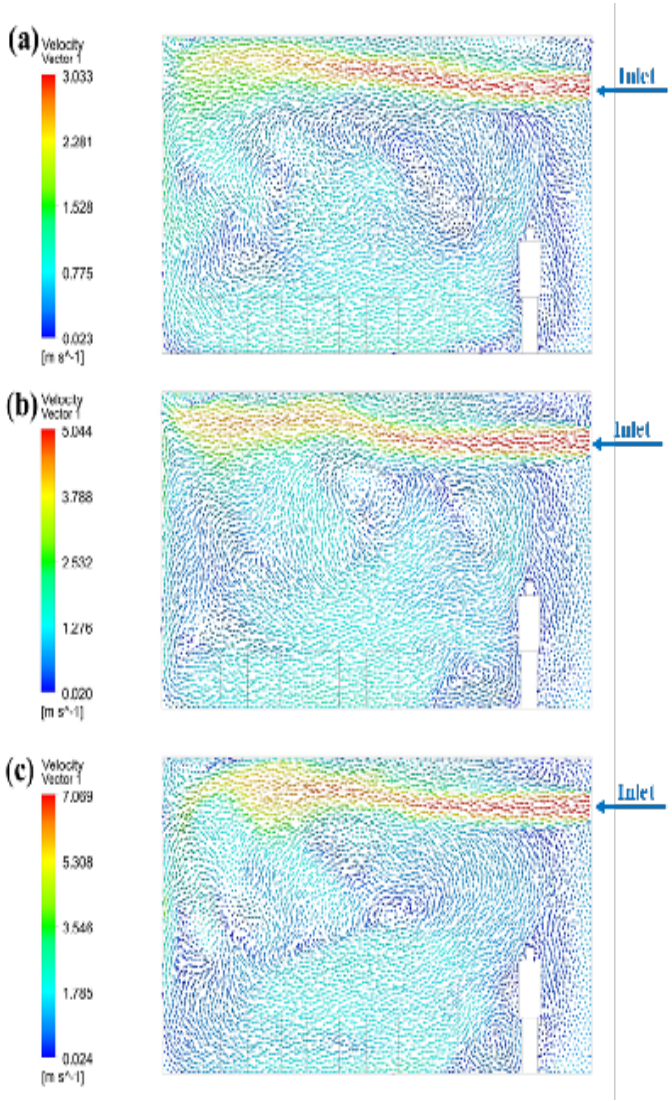

FIGURE 5. Velocity vector fields at mid-plane for side wall ventilation at different inlet velocities: (a) 3 m/s, (b) 5 m/s, and (c) 7 m/s.

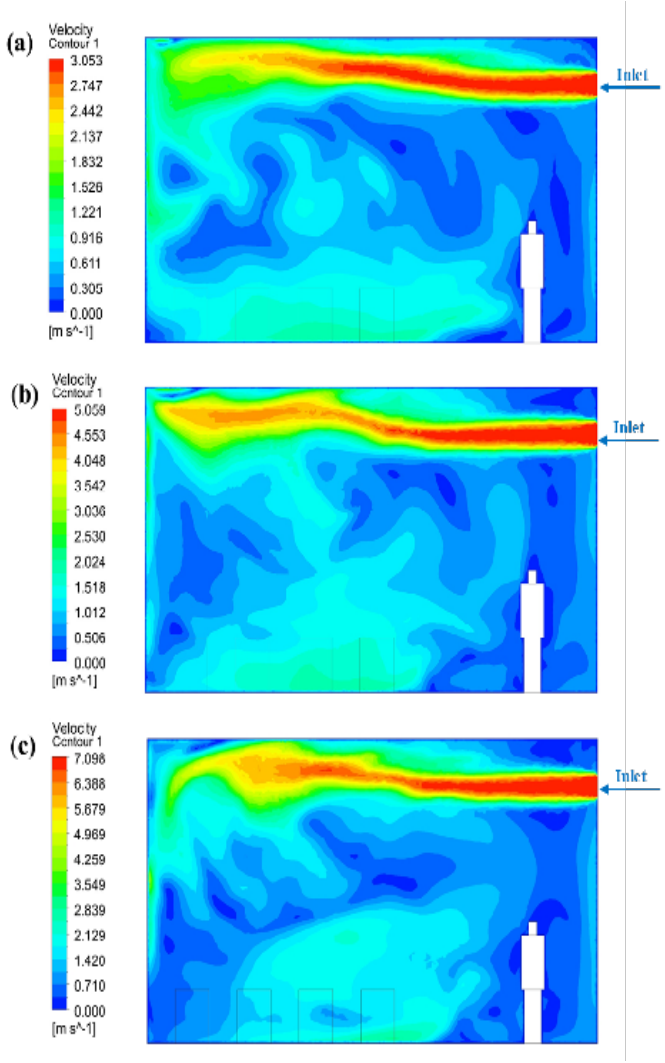

FIGURE 6. Velocity magnitude contours (in m/s) at classroom mid-plane for side wall ventilation: (a) 3 m/s, (b) 5 m/s, and (c) 7 m/s.

Particle Dispersion Under Different Ventilation Scenarios

The spatiotemporal evolution of particle distribution was evaluated under three conditions: no ventilation, top wall ventilation, and side wall ventilation. Droplet trajectories were recorded at various intervals to analyze which seating zones were most affected over time. In the absence of ventilation (Figure 12), droplets accumulate near the first row, especially in seat 3. With top ventilation, initial dispersion is limited (Figure 13); however, by 10 seconds, some particles reach seats 1–6 (Figure 14). Side ventilation shows a greater concentration near the source at 10 s (Figure 15), expanding to the rear seats, such as 22–24, after 20 s (Figure 16). After 60 s, most particles exit the classroom, but some remain near the last row (Figure 17).

DISCUSSION

This section interprets the results regarding ventilation design, airflow behavior, particle dynamics, and implications for infection risk.

Influence of Airflow Velocity on Turbulence and Jet Formation

The simulations validate the sensitivity of the velocity of the airflow against the configuration of the ventilation jet, the generation of the turbulence, and the transport of the droplets in the classroom environment. With a higher inlet velocity (7 m/s) compared to the previous velocity (3 m/s), the ventilation jets are more energetic and deeper, forming a larger and more stable circulation zone (Figures 5–8). This accelerated jet stream promotes air mixing and particles suspended, particularly along the flow axis in ventilation. In parallel, the kinetic energy of turbulence (TKE) increases significantly as the speed of airflow increases (Figures 9 and 10). It spreads the areas of turbulent mixing and promotes the wider dispersion of droplets. These findings agree with already-known principles of jet behavior in closed environments and support the existing literature by Tan and Glenn[11], Liu et al.,[9] and Kotb and Khalil,[16] who identified increased turbulent transport and possible cross-contamination with higher airspeeds in their CFD-based studies. Significantly, high turbulence not only enhances particle mixing but also causes a shorter residence time of the airborne droplets, which increases the possibility of evacuating infectious aerosols promptly. This highlights that ventilation velocity is the most crucial factor in managing the risk of air distribution within an indoor environment.

Ventilation Configuration and Spatial Exposure Risk

The spatial distribution of suspended droplets because of the ventilation layout is greatly influenced; this is the difference that is most exposed in a classroom. The top wall ventilation scheme delivers air to the ceiling and directs it downward, making the jets of air so strong at the frontmost rows of learners. In this setup, as seen in Figures 13 and 14, droplet concentration will be around seats 1–6 shortly after a coughing session.

On the other hand, the side wall ventilation type causes air to travel laterally along the room, and the direction of air moves the particles toward the back of the room as time goes on. As seen in Figures 16 and 17, the peak in the concentration of particles can be observed when it is already 20–60 s after an emission occurs, with the most in and around the last row.22–24 This redistribution effect has proved that although the top ventilation can enhance the occupants' exposure in the front row, the side ventilation can cause delayed but more extensive exposure at the back of the classroom. The results aligned with those of Abuhegazy et al.[30] who identified that ventilation's directionality significantly affects particle transport and particle deposition on a surface. The findings indicate how ventilation should be designed to be context-sensitive, with consideration to the geometrical nature of the rooms, room occupancy, floor plans, and the temporal exposure patterns.

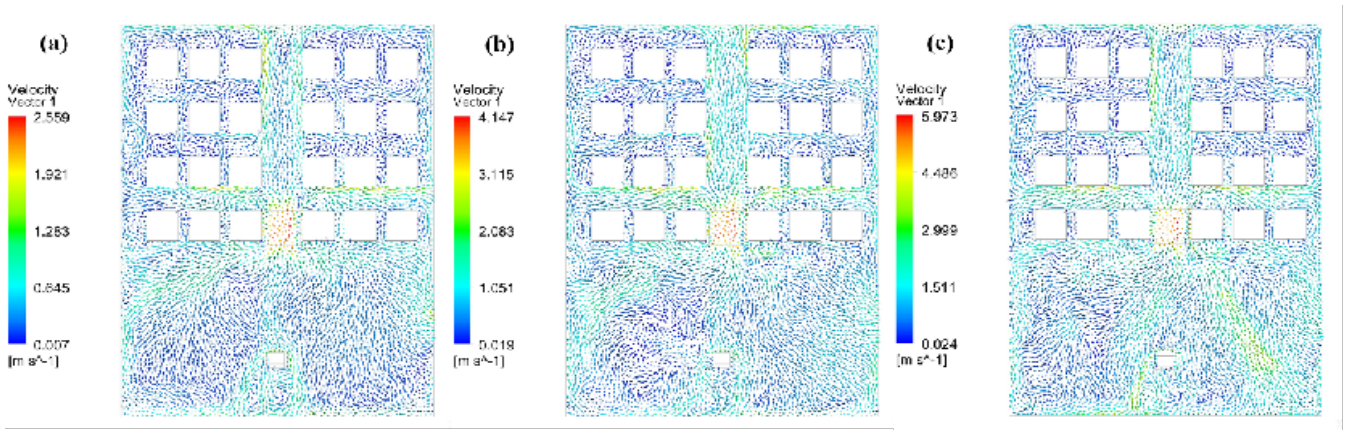

FIGURE 7. Velocity vector fields at mid-plane for top wall ventilation at inlet velocities of: (a) 3 m/s, (b) 5 m/s, and (c) 7 m/s.

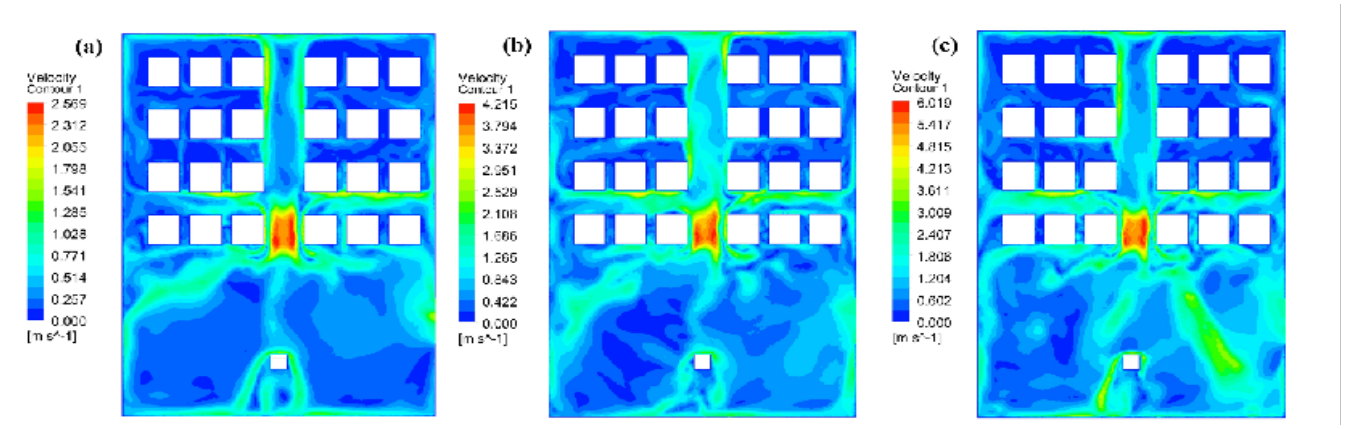

FIGURE 8. Velocity magnitude contours (in m/s) near floor level for top wall ventilation: (a) 3 m/s, (b) 5 m/s, and (c) 7 m/s.

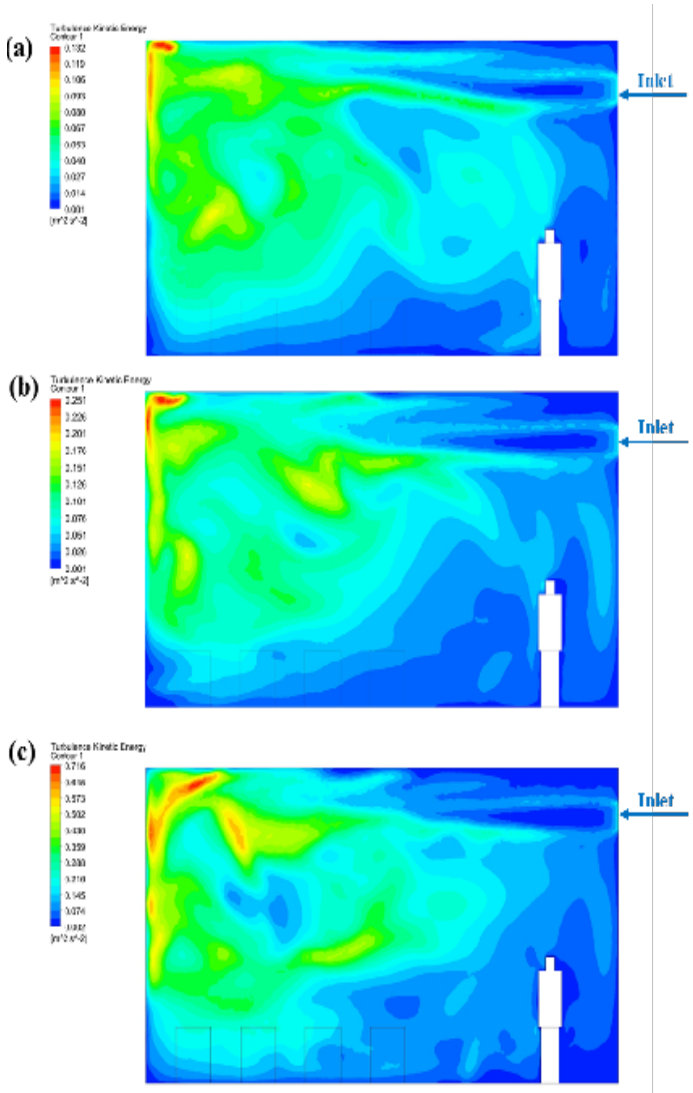

FIGURE 9. Turbulence kinetic energy (TKE) contours (in m^2/s^2) for side wall ventilation: (a) 3 m/s, (b) 5 m/s, and (c) 7 m/s.

Effect of Droplet Size on Suspension and Deposition

The size of virus-laden droplets plays a huge part in how they behave. Simulation results indicate that large droplets (100–150 µm) fall fast within a few seconds because of gravitational settling (Figure 11). These droplets are usually related to close contact and contamination of surfaces. Smaller droplets, especially those less than 1 µm across, on the contrary, can stay in the air current much longer. These particles sink to the ground a little and are more prone to be carried by wind and turbulence. This is in line with what Morawska and Milton[6] suggest in their findings, as they pointed out that aerosols are the most prominent route of transporting the transmission over long-range airborne transmission indoors. This size-dependent activity explains the significance of ventilation measures that can efficiently eliminate or dilute small particles instead of focusing on surface cleaning and spatial distancing.

Implications for Classroom Ventilation Design

Considering airflow velocity, droplet size distribution, and ventilation geometry provides interesting suggestions for improving classroom design to reduce air provision. First, it was found that the higher the ventilation velocity, the better the particle clearance, and the shorter their mean residence time (meaning that it was shortened more in the case of aerosols of small size). But this advantage should be weighed against the possibility of redistribution of particles by high-speed air to broader areas.

Secondly, the air in/out location should be well thought over. Top ventilation could quickly clear an area of particles in the breathing zone behind them, but might also cause a rise in exposure in the front seat areas. Side ventilation, however, will provide a more homogeneous air distribution in case of slow clearance or would lead to accumulation in downstream areas. This evidence confirms the approach suggested by Bazant and Bush,[8] that directional high-efficiency ventilation and an occupancy-sensitive design layout should be used. This might include not placing high-risk individuals (e.g., teachers or symptomatic students) in the direct flow path, opening air exchange rates in classrooms, and using specific filtration or air disinfection technologies.

CONCLUSION

The study examined the flow dynamics and dispersions of droplets of various sizes produced by a COVID-19-infected person coughing in a classroom with varying ventilation systems. 3D simulations were performed for various ventilation airflow velocities entering the intake

duct and exiting the open classroom door. Based on the reported findings, the following conclusions are drawn:

- Seat number 3 is the most impacted by contaminated human coughing in the absence of ventilation.
- Coughing affects the first row of students because of inadequate top ventilation. Sidewall ventilation affects the final row of students the most because of reduced airflow in that area.
- The turbulence rate rises with higher airflow velocity, increasing the dissemination of contaminated particles.
- The number of suspended droplets typically decreases as the ventilation velocity increases at a given period after injection.
- In all types of ventilation, the average concentration of droplets in the room decreases as time increases.

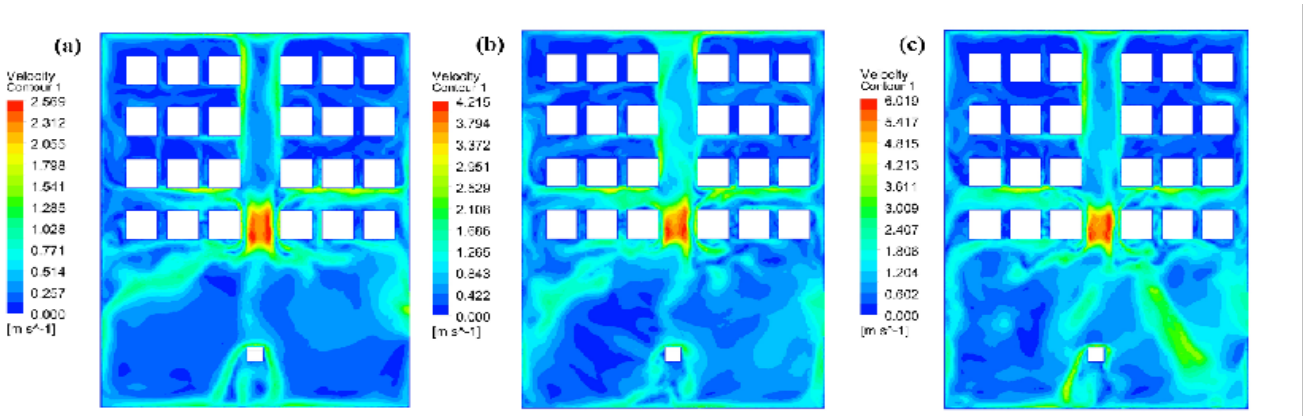

FIGURE 10. Turbulence kinetic energy (in m^2/s^2) contours for top wall ventilation: (a) 3 m/s, (b) 5 m/s, and (c) 7 m/s.

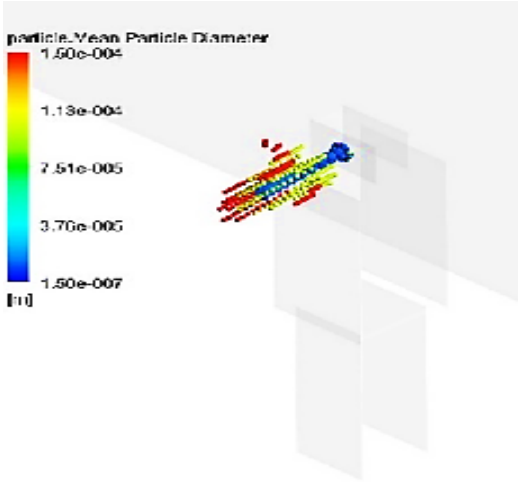

FIGURE 11. Initial droplet distribution 1 s after coughing (velocity = 10 m/s for 0.75 s): Droplets of varying diameters (0.15–150 μm).

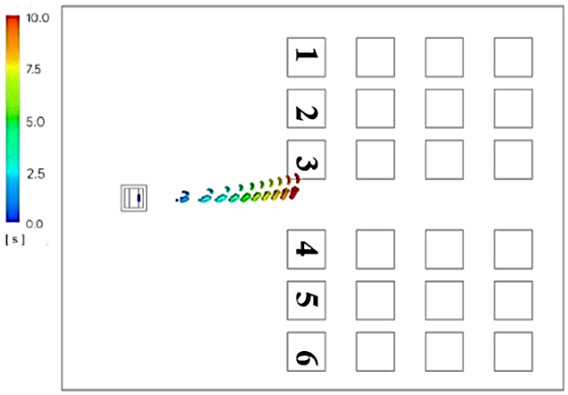

FIGURE 12. Droplet dispersion 10 s after coughing with no ventilation.

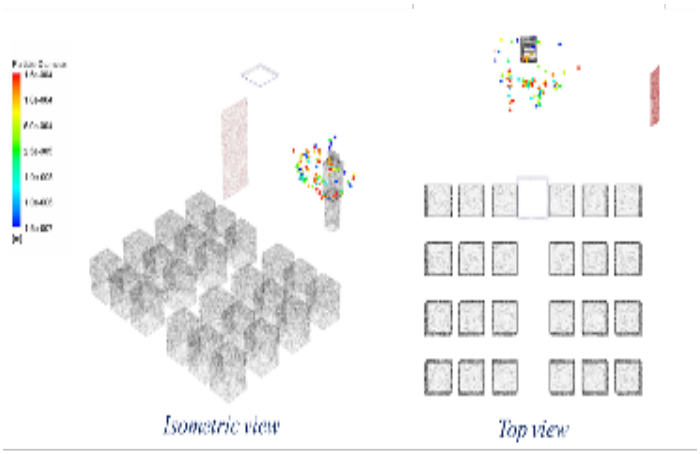

FIGURE 13. Droplet distribution 5 s after coughing with top ventilation at 5 m/s.

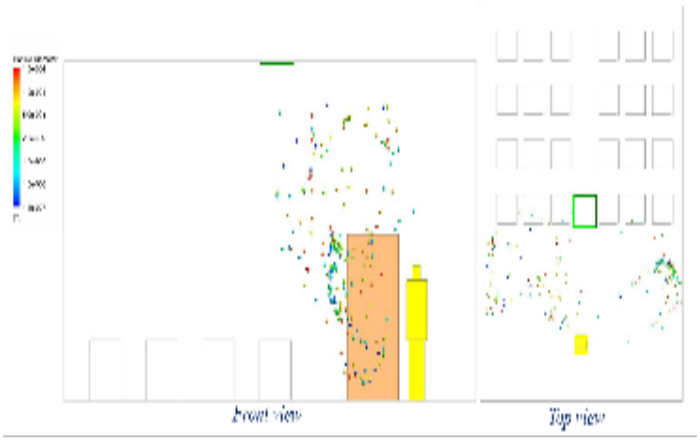

FIGURE 14. Droplet spread 10 s after coughing with top wall ventilation at 5 m/s.

FIGURE 15. Particle distribution 10 s after coughing with side wall ventilation at 5 m/s.

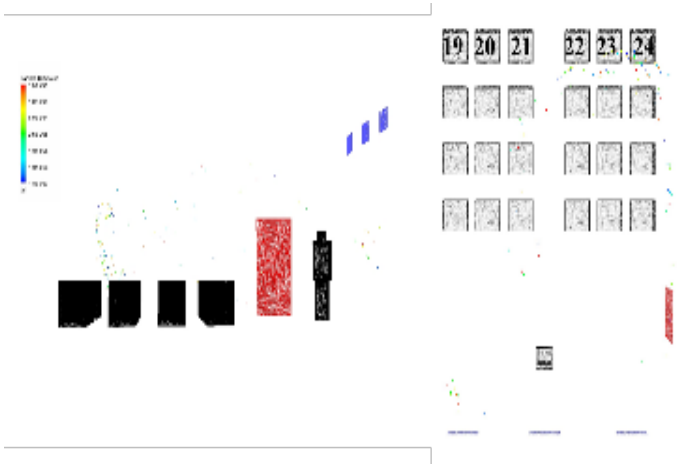

FIGURE 16. Particle distribution 20 s after coughing under side wall ventilation (5 m/s).

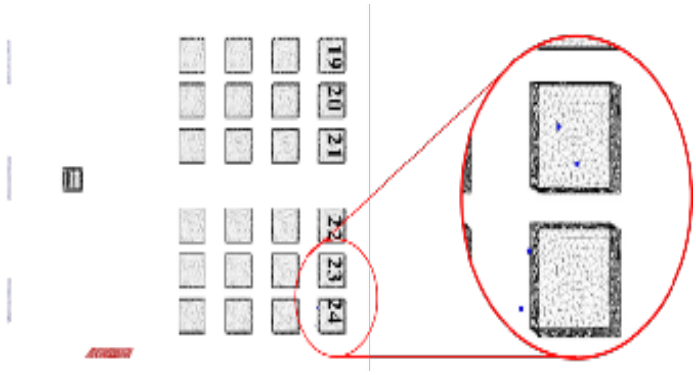

FIGURE 17. Droplet distribution 5 s after coughing with top ventilation at 5 m/s.

AUTHOR CONTRIBUTIONS

Conceptualization and methodology: A.R.P., S.K., and S.K.; Literature review: A.R.P.; Formal analysis: A.R.P. and S.K.; Writing–original draft preparation: A.R.P. and J.S.; Software: A.R.P. and S.K.; Writing–review & editing: A.R.P. and J.S.; Visualization: S.K.; Supervision: A.S., P.K., J.S., S.K.

ACKNOWLEDGMENTS

Not applicable.

FUNDING

This research received no external funding.

DATA AVAILABILITY STATEMENT

Not applicable.

CONFLICTS OF INTEREST

The authors declare they have no competing interests.

ETHICS APPROVAL AND CONSENT TO PARTICIPATE

Not applicable.

CONSENT FOR PUBLICATION

Not applicable.

FURTHER DISCLOSURE

Not applicable.

REFERENCES

1. Setti, L., Passarini, F., De Gennaro, G., et al. Potential role of particulate matter in the spreading of COVID-19 in Northern Italy: first observational study based on initial epidemic diffusion. *BMJ Open*. 2020;10:e039338. https://doi.org/https://doi.org/10.1136/bmjopen-2020-039338.
2. Xie, J. and Zhu, Y. Association between ambient temperature and COVID-19 infection in 122 cities from China. *Sci Total Environ*. 2020;724:138201. https://doi.org/10.1016/j.scitotenv.2020.138201.
3. Zu, Z.Y., Jiang, M.D., Xu, P.P., et al. Coronavirus Disease 2019 (COVID-19): A perspective from China. *Radiology*. 2020;296(2):E15–25. https://doi.org/10.1148/radiol.2020200490.
4. Ram, K., Thakur, R.C., Singh, D.K., et al. Why airborne transmission hasn't been conclusive in case of COVID-19? An atmospheric science perspective. *Sci Total Environ*. 2021;773:145525. https://doi.org/10.1016/j.scitotenv.2021.145525.
5. Wang, C.C., Prather, K.A., Sznitman, J., et al. Airborne transmission of respiratory viruses. *Science*. 2021;373(6558). https://doi.org/10.1126/science.abd9149.
6. Morawska, L. and Milton, D.K. It is time to address airborne transmission of Coronavirus Disease 2019 (COVID-19). *Clin Infect Dis*. 2020;71(9):2311–2313. https://doi.org/10.1093/cid/ciaa939.
7. Dhand, R. and Li, J. Coughs and sneezes: Their role in transmission of respiratory viral infections, including SARS-CoV-2. *Am J Respir Crit Care Med*. 2020;202(5):651–659. https://doi.org/10.1164/rccm.202004-1263PP.
8. Bazant, M.Z. and Bush, J.W.M. A guideline to limit indoor airborne transmission of COVID-19. *PNAS*. 2021;118(17). https://doi.org/10.1073/pnas.2018995118.
9. Liu, K., Allahyari, M., Salinas, J., et al. Investigation of theoretical scaling laws using large eddy simulations for airborne spreading of viral contagion from sneezing and coughing. *Phys Fluids*. 2021;33(6). https://doi.org/10.1063/5.0054651.
10. Lai, X., Li, S., Yan, J., et al. Multiphase large-eddy simulations of human cough jet development and expiratory droplet dispersion. *J Fluid Mech*. 2022;942:A12. https://doi.org/10.1017/jfm.2022.334.
11. Fabregat, A., Gisbert, F., Vernet, A., et al. Direct numerical simulation of the turbulent flow generated during a violent expiratory event. *Phys Fluids*. 2021;33(3). https://doi.org/10.1063/5.0042086.
12. von Seidlein, L., Alabaster, G., Deen, J., et al. Crowding has consequences: Prevention and management of COVID-19 in informal urban settlements. *Build Environ*. 2021;188:107472. https://doi.org/10.1016/j.buildenv.2020.107472.
13. Mao, N., An, C.K., Guo, L.Y., et al. Transmission risk of infectious droplets in physical spreading process at different times: A review. *Build Environ*. 2020;185:107307. https://doi.org/10.1016/j.buildenv.2020.107307.
14. Asadi, S., Bouvier, N., Wexler, A.S., et al. The coronavirus pandemic and aerosols: Does COVID-19 transmit via expiratory particles? *AST*. 2020;54(6):635–8. https://doi.org/10.1080/02786826.2020.1749229.
15. Diwan, S.S., Ravichandran, S., Govindarajan, R., et al. Understanding transmission dynamics of COVID-19-type infections by direct numerical simulations of cough/sneeze flows. *Trans Indian Natl Acad Eng*. 2020;5(2):255–61. https://doi.org/10.1007/s41403-020-00106-w.
16. Kotb, H. and Khalil, E.E. Sneeze and cough pathogens migration inside aircraft cabins. *REHVA J*. 2020:36–45. Availanle online: https://www.rehva.eu/rehva-journal/chapter/sneeze-and-cough-pathogens-migration-inside-aircraft-cabins.
17. Wang, J.X., Cao, X., Chen, Y.P. An air distribution optimization of hospital wards for minimizing cross-infection. *J Clean Prod*. 2021;279:123431. https://doi.org/10.1016/j.jclepro.2020.123431.
18. Zhao, Y., Sun, H., Tu, D. Effect of mechanical ventilation and natural ventilation on indoor climates in Urumqi residential buildings. *Build Environ*. 2018;144:108–18. https://doi.org/10.1016/j.buildenv.2018.08.021.
19. Wolkoff, P., Azuma, K., Carrer, P. Health, work performance, and risk of infection in office-like environments: The role of indoor temperature, air humidity, and Ventilation. *Int*

J Hyg Environ Health. 2021;233:113709. https://doi.org/10.1016/j.ijheh.2021.113709.

20. van Hooff, T., Blocken, B., Aanen, L., et al. A venturi-shaped roof for wind-induced natural ventilation of buildings: Wind tunnel and CFD evaluation of different design configurations. *Build Environ*. 2011;46(9):1797–807. https://doi.org/10.1016/j.buildenv.2011.02.009.
21. Gilani, S., Montazeri, H., Blocken, B. CFD simulation of stratified indoor environment in displacement ventilation: Validation and sensitivity analysis. *Build Environ*. 2016;95:299–313. https://doi.org/10.1016/j.buildenv.2015.09.010.
22. Barbosa, B.P.P. and Brum, N.C.L. Validation and assessment of the CFD-0 module of CONTAM software for airborne contaminant transport simulation in laboratory and hospital applications. *Build Environ*. 2018;142:139–52. https://doi.org/10.1016/j.buildenv.2018.06.013.
23. Liu, W., Liu, D., Gao, N. CFD study on gaseous pollutant transmission characteristics under different ventilation strategies in a typical chemical laboratory. *Build Environ*. 2017;126:238–51. https://doi.org/10.1016/j.buildenv.2017.09.033.
24. Ren, J., Wang, Y., Liu, Q., et al. Numerical study of three ventilation strategies in a prefabricated COVID-19 inpatient ward. *Build Environ*. 2021;188:107467. https://doi.org/10.1016/j.buildenv.2020.107467.
25. Pendarm, M.R. and Páscoa, J.C. Numerical modeling of the distribution of virus carrying saliva droplets during sneeze and cough. *Phys Fluids*. 2020;32(8). https://doi.org/10.1063/5.0018432.
26. Diwan, S.S., Ravichandran, S., Govindarajan, R., et al. Understanding transmission dynamics of COVID-19-type infections by direct numerical simulations of cough/sneeze flows. *Trans Indian Natl Acad Eng*. 2020;5(2):255–61. https://doi.org/10.1007/s41403-020-00106-w.
27. Gupta, J.K., Lin, C.H., Chen, Q. Flow dynamics and characterization of a cough. *IAQ*. 2009;19(6):517–25. https://doi.org/10.1111/j.1600-0668.2009.00619.x.
28. Liu, W., van Hooff, T., An, Y, et al. Modeling transient particle transport in transient indoor airflow by fast fluid dynamics with the Markov chain method. *Build Environ*. 2020;186:107323. https://doi.org/10.1016/j.buildenv.2020.107323.
29. Liu, W. and Chen, Q. Development of adaptive coarse grid generation methods for fast fluid dynamics in simulating indoor airflow. *J Build Perform Simul*. 2018;11(4):470–84. https://doi.org/10.1080/19401493.2017.1397195.
30. Abuhegazy, M., Talaat, K., Anderoglu, O., et al. Numerical investigation of aerosol transport in a classroom with relevance to COVID-19. *Phys Fluids*. 2020;32(10). https://doi.org/10.1063/5.0029118.
31. Bañón, L. and Bañón, C. Improving room carrying capacity within built environments in the context of COVID-19. *Symmetry (Basel)*. 2020;12(10):1683. https://doi.org/10.3390/sym12101683.
32. Shih, T.H., Liou, W.W., Shabbir, A., et al. A new k-ϵ eddy viscosity model for high reynolds number turbulent flows. *Comput Fluids*. 1995;24(3):227–38. https://doi.org/10.1016/0045-7930(94)00032-T.
33. Wang, J., Sun, L., Zou, M., et al. Bioinspired shape-memory graphene film with tunable wettability. *Sci Adv*. 2017;3(6). https://doi.org/10.1126/sciadv.1700004.
34. Verma, T.N., Sahu, A.K., Sinha, S.L. Study of particle dispersion on one bed hospital using computational fluid dynamics. *Mater Today Proc*. 2017;4(9):10074–9. https://doi.org/10.1016/j.matpr.2017.06.323.
35. Dbouk, T. and Drikakis, D. On coughing and airborne droplet transmission to humans. *Phys Fluids*. 2020;32(5):053310. https://doi.org/10.1063/5.0011960.
36. Li, A. and Ahmadi, G. Dispersion and deposition of spherical particles from point sources in a turbulent channel flow. *Aerosol Sci Technol*. 1992;16(4):209–26. https://doi.org/10.1080/02786829208959550.
37. 37.Chen, Y. and Deng, Z. Hydrodynamics of a droplet passing through a microfluidic T-junction. *J Fluid Mech*. 2017;819:401–34. https://doi.org/10.1017/jfm.2017.181.
38. 38.Zhang, C., Wu, S., Yao, F. Evaporation regimes in an enclosed narrow space. *Int J Heat Mass Transf*. 2019;138:1042–53. https://doi.org/10.1016/j.ijheatmasstransfer.2019.04.113.
39. 39.Jacob, S., Yadav, S.S., Sikarwar, B.S. Design and Simulation of Isolation Room for a Hospital. In: Saha, P., Subbarao, P., Sikarwar, B. (eds). *Advances in Fluid and Thermal Engineering. Lecture Notes in Mechanical Engineering*. 2019, Springer, Singapore. https://doi.org/10.1007/978-981-13-6416-7_8.